Research Article

Journal of MASS SPECTROMETRY

Received: 28 May 2009 Accepted: 15 July 2009 Published online in Wiley Interscience: 5 August 2009

(www.interscience.com) DOI 10.1002/jms.1625

Top–down glycolipidomics: fragmentation analysis of ganglioside oligosaccharide core and ceramide moiety by chip-nanoelectrospray collision-induced dissociation MS^2–MS^6

Alina Serb,[a,b†] Catalin Schiopu,[a†] Corina Flangea,[a,b] Eugen Sisu[b,d] and Alina D. Zamfir[a,c*]

We developed a straightforward approach for high-throughput top–down glycolipidomics based on fully automated chip-nanoelectrospray (nanoESI) high-capacity ion trap (HCT) multistage mass spectrometry (MS^n) by collision-induced dissociation (CID) in the negative ion mode. The method was optimized and tested on a polysialylated ganglioside fraction (GT1b), which was profiled by MS^1 and sequenced in tandem MS up to MS^6 in the same experiment. Screening of the fraction in the MS^1 mode indicated the occurrence of six $[M - 2H]^{2-}$ ions which, according to calculation, support 13 GT1 variants differing in their relative molecular mass due to dissimilar ceramide (Cer) constitutions. By stepwise CID MS^2–MS^5 on the doubly charged ion at *m/z* 1077.20 corresponding to a ubiquitous GT1b structure, the complete characterization of its oligosaccharide core including the identification of sialylation sites was achieved. Structure of the lipid moiety was further elucidated by CID MS^6 analysis carried out using the Y_0 fragment ion, detected in MS^5, as a precursor. MS^6 fragmentation resulted in a pattern supporting a single ceramide form having the less common (d20 : 1/18 : 0) configuration. The entire top–down experiment was performed in a high-throughput regime in less than 3 min of measurement, with an analysis sensitivity situated in the subpicomolar range.

Keywords: top–down glycolipidomics; fully automated chip-nanoESI; multistage collision-induced dissociation; ganglioside oligosaccharide sequencing; ceramide fragmentation; high throughput

Introduction

Gangliosides encompass a large family of highly complex glycosphingolipids that occur in the outer layer of the plasma membrane in all eukaryotic cells.[1–3] Gangliosides bear one or more *N*-acetylneuraminic acid (Neu5Ac) groups as branches on their hydrophilic oligosaccharide chain. The oligosaccharide core differs in the glycosidic linkage position, sugar configuration, and the content of neutral residues and sialic acid. The oligosaccharide chain is attached to a hydrophobic ceramide, which anchors the whole molecule to the plasma membrane. Ceramide moieties also vary with respect to the type of long-chain base (LCB) (sphingosine base) and *N*-linked fatty acid group. Such a structural diversity results in part from the different chain lengths, especially of the LCB, which commonly contains 18 or 20 carbon atoms. *O*-glycans are linked at C1, *N*-acylated amino group at C2, hydroxyl group at C3 and a double bond occurs between C4 and C5. Further hydroxylation and/or unsaturation of the LCB may also be present. The length of the fatty acid may vary from C16 to C26 or more, and it may be modified by the presence of one or more hydroxyl groups and points of unsaturation. While C18-LCB species are distributed in all tissues, C20-LCB species are present in significant concentrations only in the gangliosides of the central nervous system (CNS)[4–7] and their content increases throughout life.[8–10]

Gangliosides are particularly abundant in CNS and are thought to play important roles in neuritogenesis, synaptic transmission, memory formation, aging, brain development and maturation.[11–18] They also serve as mediators in intercellular recognition, adhesion and transmembrane signal transduction.[19–23]

At present, several methods exist for the determination of the ganglioside structure in various biological specimens. Antibodies to some oligosaccharide moieties are available for visualizing ganglioside species exhibiting different constitutive oligosaccharides[24]; however, currently available immunological methods cannot detect the differences in ceramide structures. On the other hand, chromatographic methods such as thin layer chromatography (TLC) and high performance liquid chromatog-

* *Correspondence to: Alina D. Zamfir, Mass Spectrometry Laboratory, National Institute for Research and Development in Electrochemistry and Condensed Matter, Plautius Andronescu Str. 1, RO-300224, Timisoara, Romania. E-mail: alina.zamfir@uav.ro*

† *These authors have contributed equally*

a *Mass Spectrometry Laboratory, National Institute for Research and Development in Electrochemistry and Condensed Matter, 300224, Timisoara, Romania*

b *Department of Biochemistry, "Victor Babes" University of Medicine and Pharmacy, 300054, Timisoara, Romania*

c *Department of Chemical and Biological Sciences, "Aurel Vlaicu" University of Arad, 310130, Arad, Romania*

d *Chemistry Institute of Romanian Academy, 300223, Timisoara, Romania*

Journal of MASS SPECTROMETRY

raphy (HPLC) that are extensively used in glycolipid research are also unable to render information on ganglioside fine structure elements.

In recent years, the continuous development of mass spectrometry (MS) strategies proficient not only in accurate molecular mass measurement but also in generating specific fragmentation of selected precursor ions has opened new perspectives in this field. Single-stage collision-induced dissociation (CID) on either quadrupole time-of-flight[25–29] or Fourier transform ion cyclotron resonance (FTICR) MS[30] were developed and applied to ganglioside structural investigation. To increase the experiment throughput, sensitivity and spray stability necessary for efficient CID MS/MS, some of these protocols included robotized sample delivery by fully automated chip-based nanoelectrospray (nanoESI).[25–27] However, in ganglioside analysis, the following limitations of single-stage fragmentation have to be mentioned: (1) in the characterization of the oligosaccharide core, a single dissociation stage in MS/MS experiments is unable to provide sufficient diagnostic ions for the assignment of all Neu5Ac positions in polysialylated species; (2) in the case of gangliosides containing atypical, usually labile modifications such as *O*-Fuc and *O*-Ac, assignment of the attachment site(s) becomes a challenging if not unfeasible task and (3) with respect to ceramide characterization, CID MS/MS of gangliosides produces only the ions corresponding to intact ceramide residue in most of the cases. Ceramide-derived fragment ions are rarely observed usually at higher CID energies when saccharide ring cleavage ions also occur and the spectrum becomes difficult to interpret.

The constraints of CID MS/MS may be overcome by multiple-stage MS (MS^n), a procedure that offers superior control of the dissociation process, better understanding of the ion fragmentation pathways and the possibility to isolate and sequence resulted product ions until the molecule structure is unequivocally determined. We have recently shown that by multistage MS up to MS^4, ganglioside oligosaccharide core could be sequenced stepwise, which made the discrimination of Neu5Ac-position isomers possible in complex mixtures from normal[31,32] and pathological[33] brain biopsies. In the past few years, a couple of studies were reported on ceramide fragmentation by triple-stage MS having intact mono- or disialylated gangliosides as initial precursors. Merrill *et al*.[34] succeeded in the MS^3 analysis of a GD1a in which fragmentation of the linked ceramide generated a spectrum supporting the rather unusual (20 : 1) sphingoid base composition in conjunction with a (18 : 0) fatty acid chain. Even more recently, in the same group, Chen *et al*.[35] applied a similar strategy and accomplished the characterization of (18 : 1/18 : 0) ceramide moiety of a GM2 component in a diseased mouse brain.

In the present study, we developed a protocol for fast and efficient top–down fragmentation of complex lipid-linked carbohydrates. The method employs fully automated chip-nanoESI (NanoMate robot) for high-throughput sample infusion in the negative ion mode in combination with high-capacity ion trap (HCT) MS^1 for screening and CID MS^2–MS^6 for fragmentation. Application of this protocol to a polysialylated ganglioside fraction allowed for the first complete characterization of the oligosaccharide chain and lipid moiety in a single experiment, which required less than 3 min of signal acquisition and analyte consumption situated in the subpicomolar range.

Experimental

Chemicals

GT1b ganglioside fraction from bovine brain was purchased as a dried powder from Sigma, Taufkirchen, Germany. An aliquot was dissolved in pure methanol to the final working concentration of 0.5 pmol/µl calculated for an average relative molecular mass (M_r) of 2000. Analytical grade methanol was purchased from Merck (Darmstadt, Germany). Prior to chip-based MS analysis, the sample/methanol solution was centrifuged for 2 h in a SIGMA 2–16 model centrifuge from Sartorius GmbH (Göttingen, Germany).

Mass spectrometry

MS was conducted on a high-capacity ion trap Ultra (HCT Ultra, PTM discovery) mass spectrometer from Bruker Daltonics (Bremen, Germany) controlled by Compass™ 1.2 integrated software package. All mass spectra were acquired in the mass range of 100–2800 *m/z*, with a scan speed of 8000 *m/z*/s. MS^2–MS^6 was carried out by CID using He as the collision gas. For multistage sequencing, the precursor ions were selected within an isolation width of 2 u. Fragmentation spectra were obtained by accumulating scans at variable rf signal amplitudes within 0.6–1.0 V.

All mass spectra were calibrated using G2421A electrospray 'tuning mix' from Agilent Technologies (Santa Rosa, CA, USA) as external calibrant. The reference provided a spectrum with a fair ionic coverage of the *m/z* range scanned in both MS and CID MS^n experiments in the negative ion mode. The obtained mass accuracy was situated within the normal range of an HCT MS instrument.

Data analysis and interpretation of mass spectra

All total ion chromatograms and derived mass spectra were processed by Data Analysis 3.4. software portal from Bruker Daltonics (Bremen, Germany).

The assignment of molecular ions to a certain composition was made by exact mass calculation, while the postulation of oligosaccharide core structures and linkages was based on the previously acquired information[25–30] and ganglioside biosynthesis pathway principles.

The assignment of oligosaccharide sequence ions followed the generally accepted nomenclature introduced by Domon, Costello[36] and revised by Costello *et al*.[37] Ceramide fragment ions were assigned according to the nomenclature of Ann and Adams.[38]

Fully automated chip-based nanoelectrospray

Fully automated chip-based nanoelectrospray was performed on a NanoMate robot incorporating ESI 400 Chip technology (Advion BioSciences, Ithaca, USA) controlled and manipulated by ChipSoft 8.1.0 software operating under Windows system. The robot was coupled to the HCT Ultra mass spectrometer via an in-laboratory made mounting system as described by us earlier.[32,33]

Five microliters of aliquot of the working sample solution was loaded into the NanoMate 96-well plate. The robot was tuned for operating in the negative ion mode and programmed to aspirate the whole volume of sample, followed by 2 µl of air into the pipette tip and afterward deliver the sample to the inlet side of the 400 microchip. The electrospray process was initiated by applying a voltage of −0.90 kV on the pipette tip, and 0.40 p.s.i. nitrogen

back pressure. In order to eliminate the in-source cleavage of labile Neu5Ac groups as much as possible, after electrospray initiation, the voltage applied onto the pipette tip was gradually reduced down to −0.7 kV and the spray was maintained by increasing the nitrogen back pressure up to 0.60 p.s.i. A voltage of −0.7 kV at 0.60 p.s.i. gas pressure represented the minimal voltage value for which a stable spray could be maintained throughout the MS^1–MS^6 experiment. To further reduce the in-source fragmentation, the HCT capillary exit was set to a low value of −50 V. The source block maintained at a constant temperature of 150 °C provided an optimal desolvation of the generated droplets without the need of desolvation gas. Each chip nozzle had an internal diameter of 2.5 µm, which, under the given conditions, delivered a working flow rate of approximately 50 nl/min.

Results and Discussion

Assessment of GT1b fraction composition by chip-based nanoESI MS screening

Fully automated chip-based nanoESI MS^1 screening of the commercially available GT1b fraction from bovine brain isolated by TLC acquired for only 30 s is depicted in Fig. 1. Considering only the ubiquitous ceramide forms, 29 gangliosides of which 13 GT1 species differing in either oligosaccharide or ceramide composition were identified by MS^1 through their detected $[M - 2H]^{2-}$ ions. The ion assignment and structure postulation was made according to *m/z* measurement followed by M_r calculation as presented in Table 1. Figure 1 shows that the most abundant ions correspond to GT1 (d18 : 1/20 : 0), (d18 : 0/20 : 1) and/or (d20 : 0/18 : 1), (d20 : 1/18 : 0) detected at *m/z* 1077.20, followed by GT1 (d18 : 1/18 : 0) and/or (d18 : 0/18 : 1) at *m/z* 1063.20. The presence of three minor GT1 molecular species is documented by the ion signals of rather low intensity at *m/z* 1049.25, 1085.20 and 1088.20, which can be assigned by calculation to GT1 (d18 : 1/16 : 0) and/or (d18 : 0/16 : 1), GT1 (d18 : 0/21 : 0) and GT1(d18 : 1/22 : 2) and/or GT1(d18 : 0/22 : 3) respectively.

Interestingly, six GT2-, two GD3- and six GD1-type of species were also detected as ions of lower relative abundance. The disialylated GD1 could arise as either components in the mixture or as products of in-source fragmentation resulting from the

Table 1. Assignment according to calculated M_r of the major ions detected in the screening mass spectrum presented in Fig. 1

m/z	Type of ion	Proposed ion composition
717.80	$[M - 2H]^{2-}$	GD3(d18 : 1/16 : 3); GD3(d18 : 0/16 : 4)
917.60	$[M - 2H]^{2-}$	GD1(d18 : 0/18 : 0)*
926.63	$[M + Na - 3H]^{2-}$	GT3(d18 : 1/23 : 0); GT3(d18 : 0/23 : 1)
931.72	$[M - 2H]^{2-}$	GD1(d18 : 1/20 : 0); GD1(d18 : 0/20 : 1); GD1(d20 : 0/18 : 1)
939.60	$[M - 2H]^{2-}$	GD1(d18 : 1/21 : 0); GD1(d18 : 0/21 : 1)
1020.16	$[M - 2H]^{2-}$	GT2(d18 : 1/24 : 4); GT2(d18 : 0/24 : 5)
1033.36	$[M - 2H]^{2-}$	GT2(d18 : 0/22 : 0)
1049.25	$[M - 2H]^{2-}$	GT1(d18 : 1/16 : 0); GT1(d18 : 0/16 : 1)
1063.20	$[M - 2H]^{2-}$	GT1(d18 : 1/18 : 0)* ; GT1(d18 : 0/18 : 1)*
1071.20	$[M - 2H]^{2-}$	GT2(d18 : 1/31 : 2); GT2(d18 : 0/31 : 3)
1074.20	$[M - 2H]^{2-}$	GT2(d18 : 0/31 : 0)*
1077.20	$[M - 2H]^{2-}$	GT1(d18 : 1/20 : 0); GT1(d18 : 0/20 : 1) GT1(d20 : 0/18 : 1); GT1(d20 : 1/18 : 0)*
1085.20	$[M - 2H]^{2-}$	GT1(d18 : 0/21 : 0)
1088.20	$[M - 2H]^{2-}$	GT1(d18 : 1/22 : 2); GT1(d18 : 0/22 : 3)
1098.20	$[M - 2H]^{2-}$	GT1(d18 : 1/23 : 0); GT1(d18 : 0/23 : 1)

The structures marked by * were validated by CID multistage MS.

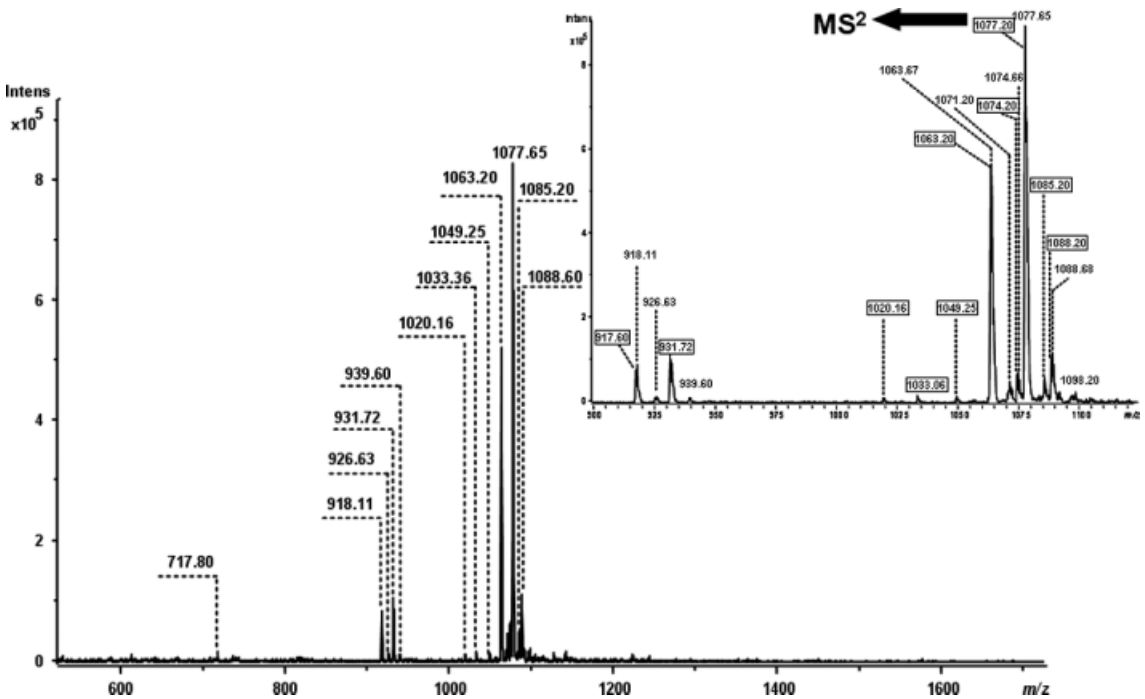

Figure 1. Fully automated (−) nanoESI chip HCT MS^1 of the standard GT1b fraction. Solvent: MeOH; sample concentration: 0.5 pmol/µl; acquisition time: 30 s; Chip ESI: −0.7 kV; capillary exit: −50 V. Only the most ubiquitous ceramide forms were considered. Inset: zoomed (900–1100) *m/z* area with highlighted monoisotopic values.

Journal of MASS SPECTROMETRY

cleavage of one sialic acid residue from the intact trisialylated GT1 components. According to the intensity of the signals assigned to disialylated GD1 ions, only a low level of in-source fragmentation occurs during the MS^1 ionization process. Neu5Ac residue linked to the terminal Gal as a monosialo group is known to be more susceptible to enzymatic cleavage. Loss of the Neu5Ac bound to the inner Gal would produce a high extent of disialo ions along with the occurrence of GM1-like fragment ions, which are not detectable in the spectrum. Moreover, the employed mild ionization conditions, the significantly lower extent of in-source induced fragmentation reported previously[25–27,32,33] in relation to chip-based ESI as well as the presence of GT2 and GD3, which cannot be attributable to in-source decay, corroborate the GD1 incidence in the investigated fraction.

Because MS^1 cannot disclose information related to the molecular structure, as observable in the molecular ion list, only the most common lipid variants were assigned to a certain M_r value at this stage of analysis. According to the determined M_r, all ceramide residues exhibit a dihydroxylated sphingoid base and differ in fatty acid or sphingoid base composition, number and position of the double bonds.

Sequencing of GT1b oligosaccharide core by CID MS^2–MS^5

To test the feasibility of a top–down experiment for polysialylated ganglioside species, the doubly deprotonated ion at *m/z* 1077.20 corresponding, according to calculation, to a ubiquitous GT1 form known to contain mostly ceramide of (d18:1/20:0) or (d18:0/20:1) compositions was isolated within an isolation window of 2 u and submitted to stepwise fragmentation by low energy multistage CID. MS^2–MS^5 analysis of this precursor ion is depicted in Figs 2–4 together with the corresponding schemes illustrating the path of fragmentation experienced by the precursor ions during each dissociation phase.

Because of the Neu5Ac labile linkage, the most important process induced by the first fragmentation stage (MS^2) is molecule desialylation (Fig. 2(a) and (b)). Detachment of one terminal Neu5Ac is documented by the abundant fragment ions $Y_{4\alpha}^-$ and $Y_{3\beta}^-$ at *m/z* 1864.21 and $Y_{4\alpha}^{2-}$ and $Y_{3\beta}^{2-}$ at *m/z* 932.10 that are accompanied by their afferent dehydrated counterparts $Z_{4\alpha}^-$ and $Z_{3\beta}^-$ at *m/z* 1846.27. In this context, it is necessary to note that basically MS sequencing cannot render fragment ions that are exclusive diagnostic for Neu5Ac attachment at outer galactose because of the symmetry of the Gal-GalNAc-Gal chain. For this reason, and having in view that MS screening also indicated the presence of other ganglioside species, we cannot exclude the possible incidence of GT1a in the mixture. Therefore, on the spectra sialylated product ions that might arise from both a and b series were labeled with the corresponding dual assignment.

The subsequent loss of Neu5Ac and/or the direct cleavage of two Neu5Ac residues is confirmed by the abundant $Y_{2\beta}^-$ and $Y_{4\alpha}/B_{1\beta}^-$ at *m/z* 1573.21 and $Z_{2\beta}^-$ and $Y_{4\alpha}/C_{1\beta}^-$ at *m/z* 1555.20, while the double cleavage and complete Neu5Ac elimination is documented by the less abundant asialo $Y_{4\alpha}/B_{2\beta}^-$ fragment ion at *m/z* 1282.06. The ions at *m/z* 537.40 and 581.32 are also

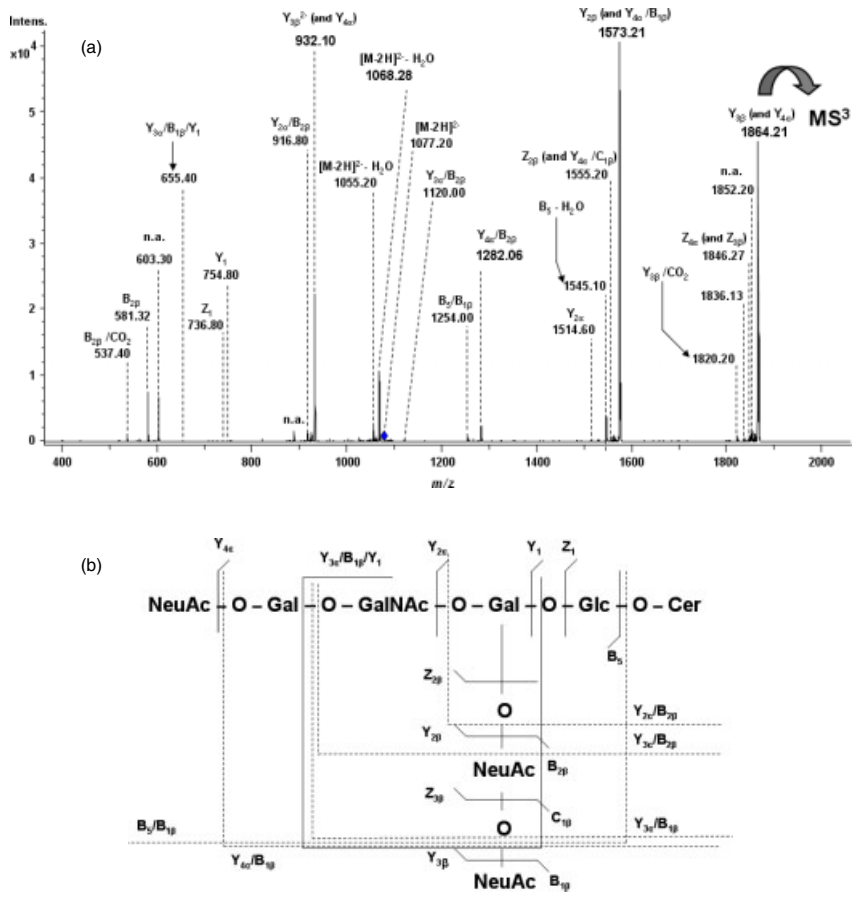

Figure 2. (a) CID MS^2 of the doubly charged ion at *m/z* 1077.20; (b) ion structure and fragmentation scheme corresponding to b ganglioside series. Acquisition time: 30 s; variable rf signal amplitudes within 0.6–1.0 V; n.a. – not assigned.

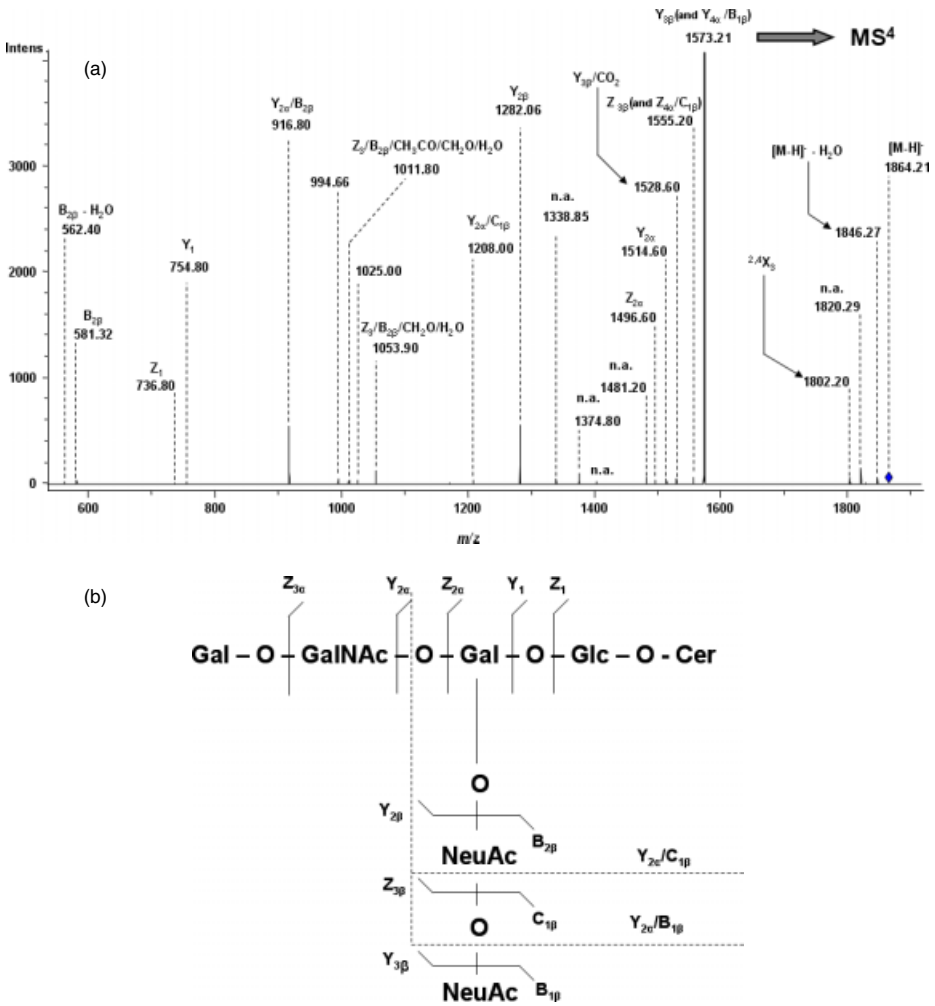

Figure 3. (a) CID MS^3 of $[M-H]^-$ ion at *m/z* 1864.21 corresponding to $Y_{3\beta}{}^-$ and $Y_{4\alpha}{}^-$ fragment ion detected in MS^2. (b) Ion structure and fragmentation scheme corresponding to b ganglioside series. Acquisition time: 30 s; variable rf signal amplitudes within 0.6–1.0 V; n.a. – not assigned.

indicative of the extensive desialylation process induced by MS^2 fragmentation. They correspond to $B_{2\beta}{}^-$ after neutral loss of CO_2 ($Neu5Ac_2{}^-/CO_2$) and $B_{2\beta}{}^-$ ($Neu5Ac_2{}^-$).

The spectrum in Fig. 2(a) exhibits only a few ions resulting from cleavage of glycosidic bonds other than that of Neu5Ac. These ions are mostly those characterizing a part of the sequence at the reducing end such as $Y_{2\alpha}{}^-$ at *m/z* 1514.60 and $Y_1{}^-$ and $Z_1{}^-$ at *m/z* 754.80 and 736.80 respectively. An interesting aspect is that on one side $B_{2\beta}{}^-$ and $Y_{2\alpha}{}^-$ indicate that the Neu5Ac–Neu5Ac element exists and on the other that it is possibly linked to the inner Gal, which would indeed correspond to a GT1b type of isomer.

To confirm this concept, the disialylated singly charged ion at *m/z* 1864.21 having a GD1 (d18 : 1/20 : 0) or (d18 : 0/20 : 1)-like composition and corresponding to $Y_{4\alpha}{}^-$ and $Y_{3\beta}{}^-$ fragment ions in MS^2 was isolated and submitted to the MS^3 experiment. The resulting spectrum and fragmentation pathway are presented in Fig. 3(a) and (b). The most abundant fragment ions demonstrate a stepwise stripping of labile Neu5Ac residues, desialylation being again the major dissociation process. $Y_{3\beta}{}^-$ and $Y_{4\alpha}/B_{1\beta}{}^-$ at *m/z* 1573.21 and $Z_{3\beta}{}^-$ and $Z_{4\alpha}/C_{1\beta}{}^-$ at *m/z* 1555.20 ions are typical for monodesialylation, while the pair $B_{2\beta}{}^-$ at *m/z* 581.32 and $Y_{2\beta}{}^-$ counterpart at *m/z* 1282.06 document the cleavage of both Neu5Ac moieties and therefore complete desialylation.

The disialylated ions $Y_{2\alpha}{}^-$ and $Z_{2\alpha}{}^-$ at *m/z* 1514.60 and 1496.60 respectively, together with $B_{2\beta}{}^-$, indicate that one of the ions chosen as precursor in MS^3 contains the disialo element and this element is attached to the inner Gal. Thus, one variant of GD1-like fragment ion resulted from GT1 precursor after cleavage at stage MS^2 of the Neu5Ac moiety originally linked to the outer Gal.

Auxiliary data confirming this fragmentation pathway and sites of sialylation were obtained in an MS^4 experiment carried out using GM1 (d18 : 1/20 : 0) or (d18 : 0/20 : 1)-like $Y_{3\beta}{}^-$ and $Y_{4\alpha}/B_{1\beta}{}^-$ fragment ion detected in MS^3 at *m/z* 1573.21 as the precursor. Likewise, the ion was isolated within an isolation window of 2 u and submitted to CID using fragmentation amplitudes ranging from 0.6 to 1.0 V. MS^4 and the allied ion fragmentation proposals are presented in Fig. 4(a) and (b). In contrast to MS^2–MS^3, the advanced MS^4 stage of fragmentation applied to the smaller monosialotetraose fragment gave rise to a rich fragmentation pattern and a number of product ions that characterize the carbohydrate sequence completely (Fig. 4(a)). The generation of $Neu5AcGalGlcCer^-$ detected at *m/z* 1207.40 as $Y_{2\alpha}{}^-$ and $GalNAc(Neu5Ac)GalGlcCer^-$ detected at *m/z* 1408.80 as $Y_{3\alpha}{}^-$ ions of fair relative abundance is of high relevance. These ions substantiate Neu5Ac attachment site at the inner Gal of monosialotetraose fragment. The process of exhaustive desialylation is supported by the presence of $Y_{3\alpha}/C_{1\beta}{}^-$ and

Journal of MASS SPECTROMETRY

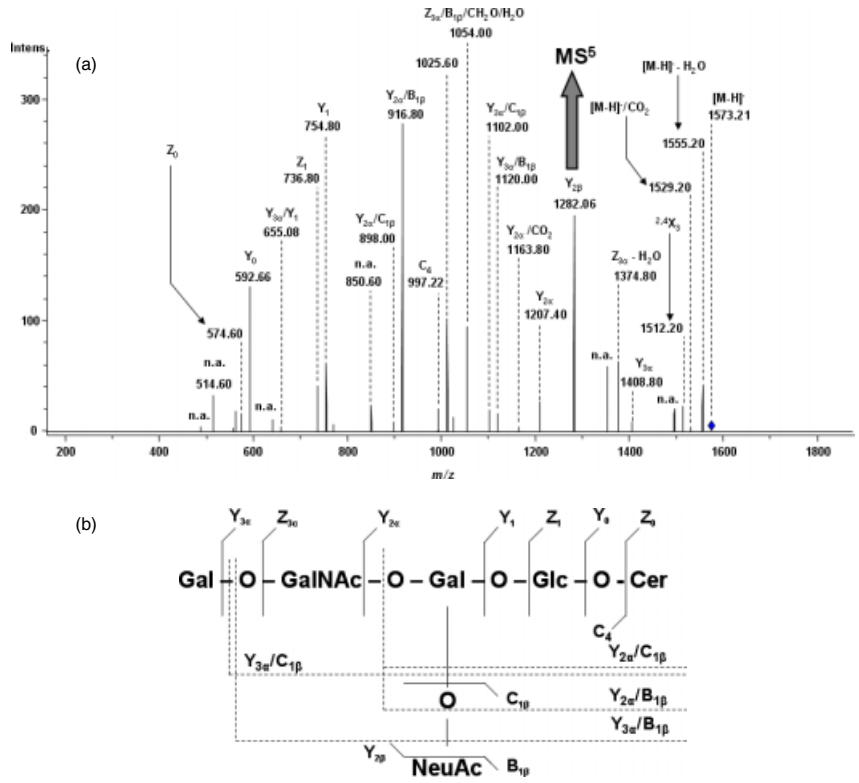

Figure 4. (a) CID MS^4 of $[M - H]^-$ ion at *m/z* 1573.21 corresponding to $Y_{3\beta}^-$ and $Y_{4\alpha}^-/B_{1\beta}^-$ fragment ion detected in MS^3. (b) Ion structure and fragmentation scheme corresponding to b ganglioside series. Acquisition time: 30 s; variable rf signal amplitudes within 0.7–0.9 V; n.a. – not assigned.

$Y_{3\alpha}/B_{1\beta}^-$ fragment ions at *m/z* 1102.00 and 1120.00 together with GalGalNAcGalGlcCer$^-$ sequence ion detected at *m/z* 1282.06 as $Y_{2\beta}^-$.

In Fig. 5, MS^5 fragmentation analysis of asialo $Y_{2\beta}^-$ ion detected at *m/z* 1282.06 in MS^4 is presented. This sequencing stage was carried out in order to confirm the oligosaccharide backbone structure. As visible in the accompanying fragmentation scheme (inset Fig. 5), the signals at *m/z* 1101.80, 916.60, 754.80 and 736.80 correspond to Z_3^-, Y_2^-, Y_1^- and Z_1^- set of product ions, which characterize the linear GalGalNAcGalGlc motif completely.

Fragmentation of GT1b ceramide residue by CID MS^6

In the spectrum in Fig. 5, a signal was observed at *m/z* 592.66 that documents the intact ceramide detachment as a negative ion in addition to the ions related to the saccharide backbone cleavage. To evaluate the ceramide composition and complete the top–down fragmentation protocol, this ion assigned to Y_0^- (Cer) was isolated within an isolation window of 2u and subjected to fragmentation in the CID MS^6 experiment. The obtained fragmentation spectrum is presented in Fig. 6. Although in such an advanced stage of CID the low absolute intensity of the precursor ion leads to a reduced fragment ion yield, the spectrum in Fig. 6 indicates that in only 10 s of signal acquisition seven well-distinguishable product ions were generated.

Three of them appear to be related to ceramide cleavages, while the other two occur after neutral elimination of small molecules from the intact precursor through a mechanism discussed by us below. To facilitate the distinction of assigned ions in Fig. 6, a general fragmentation scheme that includes the detected fragment ions and their nomenclature is given as inset.

The ions at *m/z* 265.80, 283.40 and 308.80 are diagnostic for a ceramide configuration having a dihydroxylated sphingoid base with 20 carbon atoms and one double bond and a fatty acid chain consisting of 18 carbon atoms bearing no double bond (inset Fig. 6). Thus, according to mass calculation, the ion at *m/z* 265.80 is consistent with the P-type of fragment ion characteristic for (d20 : 1) sphingoid base, which was generated via a mechanism depicted in Fig. 7(a). The ions at *m/z* 283.40 and 308.80 are diagnostic for a (d18 : 0) fatty acid chain and correspond to V+16 and T fragment ions respectively. The formation mechanism of the V+16 fragment and rearrangement ion as well as of T fragment ion is presented in Fig. 7(b).

Besides the ions discussed above, two additional signals at *m/z* 327.60 and 339.20 were detected in the same (200–400) *m/z* range, as visible in the spectrum in Fig. 6. These signals could not be attributed to any Cer (d20 : 1/18 : 0)-related cleavages, therefore they either represent rearrangement ions yet unidentified or arise as electronic noise in the ion trap.

The two ions at 544.60 and 562.60 resulting after small molecule elimination further support the composition of the precursor ion. The ion at *m/z* 562.60 arises from the precursor via an alcohol-specific α-cleavage leading to the loss of formaldehyde molecule. Further on, as an aliphatic hydroxylated species, the ion at *m/z* 562.60 undergoes the characteristic process of water elimination, which leads to the formation of the ion at *m/z* 544.60.

Conclusions

A powerful and straightforward methodology for top–down glycolipidomics was developed and optimized here for the analysis of polysialylated gangliosides. The method involves

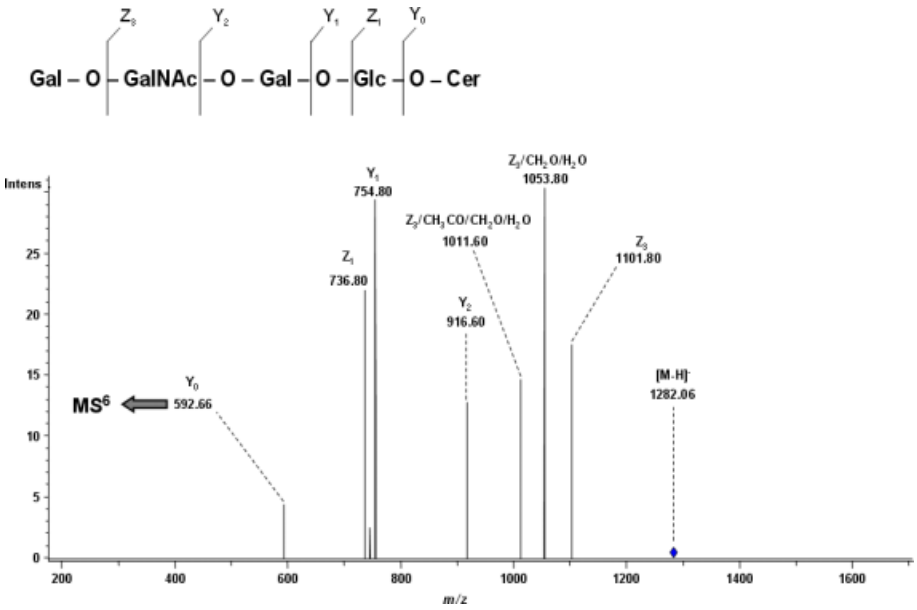

Figure 5. CID MS^5 of $[M - H]^-$ ion at *m/z* 1282.06 corresponding to $Y_{2\beta}^-$ fragment detected in MS^4. Acquisition time: 30 s; variable rf signal amplitudes within 0.6–0.8 V. Inset: ion structure and fragmentation scheme.

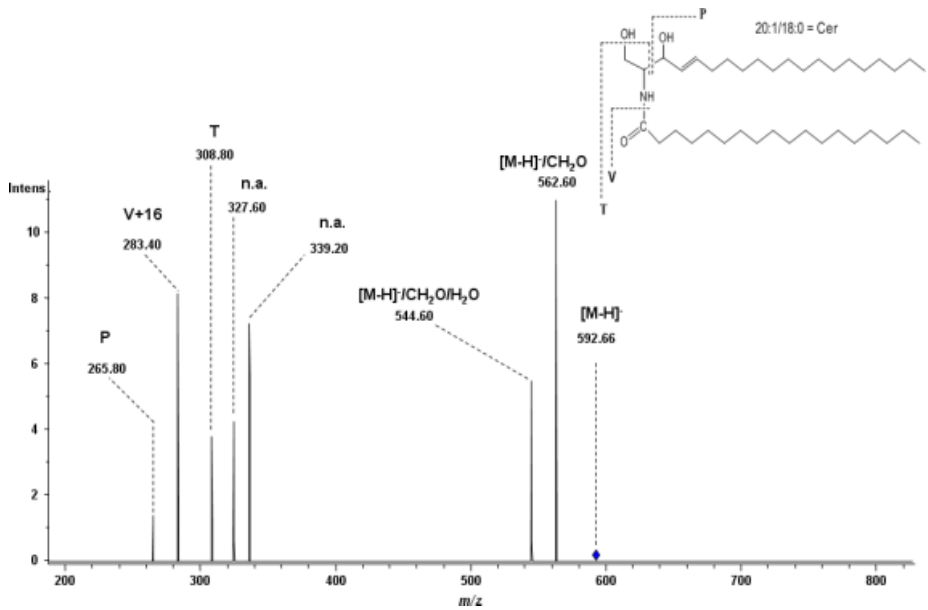

Figure 6. CID MS^6 of $[M - H]^-$ ion at *m/z* 592.66 corresponding to Y_0^- detected in MS^5. Acquisition time: 10 s; variable rf signal amplitudes within 0.4–0.6 V. Inset: general fragmentation scheme of (d20 : 1/18 : 0) ceramide variant supported by CID MS^6. Nomenclature of detected fragment ions is according to Adams and Ann;[38] n.a. – not assigned.

fully automated negative ion mode chip-based nanoelectrospray for sample infusion into a HCT mass spectrometer followed by multistage fragmentation using CID at low energies up to MS^6.

The feasibility of this approach was tested for top–down sequencing of a commercially available trisialylated ganglioside fraction from bovine brain. According to the specifications of the producer, the sample should have contained GT1b species isolated by TLC. Six molecular ions correlated to 13 GT1 species were detected by MS^1 screening in addition to other types of ganglioside components, identified as GD1, GT2 and GD3. As GT2 and GD3 cannot originate from in-source fragmentation or be considered possible artifacts induced by MS experiment, their detection in the first stage of MS analysis is attributable to the limited TLC separation efficiency.

The ion corresponding to GT1b species having the experimentally determined M_r 2156.40 was chosen as a precursor in the top–down fragmentation analysis up to the MS^6 stage. Within MS^2–MS^5 dissociation events, a complete characterization of the oligosaccharide core including discrimination of sialylation sites was achieved by stepwise sequencing of tri-, di-, mono- and finally asialo fragment ions. Further, the lipid moiety was structurally characterized by CID MS^6 performed on its corresponding ion detected as an Y_0^- fragment at the MS^5 stage. Although GT1 (d18 : 1/20 : 0) and (d18 : 0/20 : 1) forms are most frequently expressed, obtained

Journal of MASS SPECTROMETRY

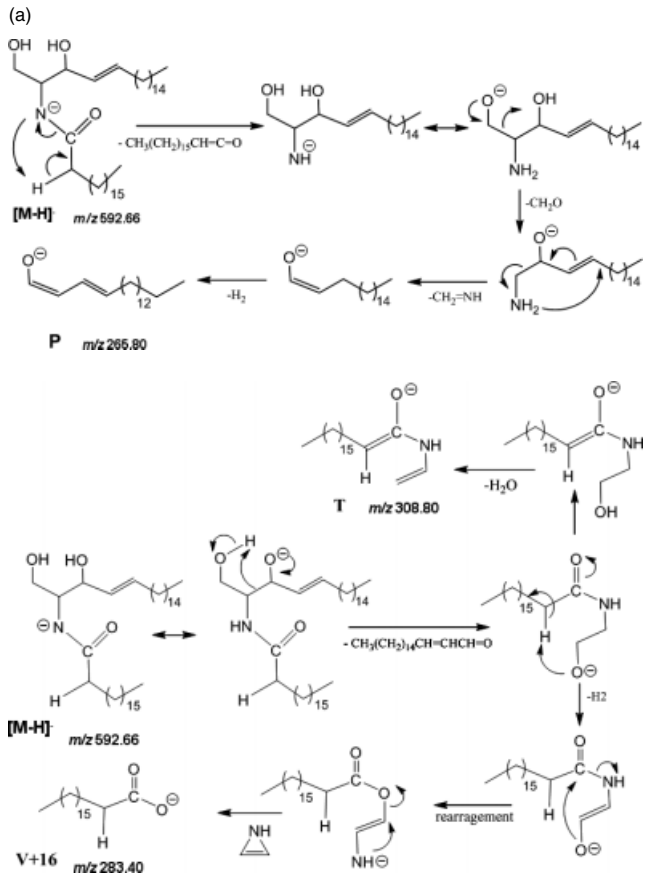

Figure 7. Fragmentation mechanism of $[M - H]^-$ ion at *m/z* 592.66 illustrating the formation of (a) P ion at *m/z* 265.80; (b) T and V+16 ions at *m/z* 308.80 and 283.40.

MS^6 product ions and fragmentation pathway(s) supported a less common ceramide variant, having the constitution (d20 : 1/18 : 0).

MS^1–MS^6 were performed in a single experiment in a high-throughput mode within a total acquisition time of only 2.66 min. In view of the flow rate provided by NanoMate chip technology, the employed solvent and working sample concentration, we estimate that only 0.133 pmols of material was used for the entire top–down experiment. Consequently, we succeeded in designing the first top–down approach applicable to glycolipidomics surveys at subpicomolar range of sensitivity that is functional in the high-throughput mode without the need of additional separation techniques on-line coupled to MS.

Acknowledgements

This work was supported by the Romanian National Authority for Scientific Research (ANCS) through the grant PN-II-41001/2007.

References

[1] L. Svennerholm. The quantitative estimation of cerebrosides in nervous tissue. *Journal of Neurochemistry* **1956**, *1*, 142.
[2] R. Ledeen, R. K. Yu. Gangliosides: structure, isolation, and analysis. *Methods in Enzymology* **1982**, *83*, 139.
[3] L. Cantù, M. Corti, P. Brocca, E. Del Favero. Structural aspects of ganglioside-containing membranes. *Biochimica et Biophysica Acta* **2009**, *1788*, 202.
[4] S. Sonnino, V. Chigorno. Ganglioside molecular species containing C18- and C20-sphingosine in mammalian nervous tissues and neuronal cell cultures. *Biochimica et Biophysica Acta* **2000**, *1469*, 63.
[5] K. Sambasivarao, R. H. McCluer. Lipid components of gangliosides. *Journal of Lipid Research* **1964**, *15*, 103.
[6] H. P. Schwarz, I. Kostyk, A. Marmolejo, C. Sarappa. Long-chain bases of brain and spinal cord of rabbits. *Journal of Neurochemistry* **1967**, *14*, 91.
[7] F. B. Jungalwala, V. Hayssen, J. M. Pasquini, R. H. McCluer. Separation of molecular species of sphingomyelin by reversed-phase high-performance liquid chromatography. *Journal of Lipid Research* **1979**, *20*, 579.
[8] P. Palestini, S. Sonnino, G. Tettamanti. Lack of the ganglioside molecular species containing the C20-long-chain bases in human, rat, mouse, rabbit, cat, dog, and chicken brains during prenatal life. *Journal of Neurochemistry* **1991**, *56*, 2048.
[9] P. Palestini, M. Masserini, S. Sonnino, A. Giuliani, G. Tettamanti. Changes in the ceramide composition of rat forebrain gangliosides with age. *Journal of Neurochemistry* **1990**, *54*, 230.
[10] R. K. Yu, Y. Nakatani, M. Yanagisawa. The role of glycosphingolipid metabolism in the developing brain. *Journal of Lipid Research* **2009**, *50*, S440.
[11] H. Rahmann. Brain gangliosides and memory formation. *Behavioural Brain Research* **1995**, *66*, 105.
[12] A. Prinetti, K. Iwabuchi, S. Hakomori. Glycosphingolipid-enriched signaling domain in mouse neuroblastoma Neuro2a cells. Mechanism of ganglioside-dependent neuritogenesis. *The Journal of Biological Chemistry* **1999**, *274*, 20916.
[13] O. A. Ramirez, R. A. Gomez, H. F. Carrer. Gangliosides improve synaptic transmission in dentate gyrus of hippocampal rat slices. *Brain Research* **1990**, *506*, 291.
[14] M. Kotani, T. Terashima, T. Tai. Developmental changes of ganglioside expressions in postnatal rat cerebellar cortex. *Brain Research* **1995**, *700*, 40.
[15] S. E. Carlson. Early determinants of development: a lipid perspective. *The American Journal of Clinical Nutrition* **2009**, *89*, 1523S.
[16] S. Hakomori. Tumor-associated carbohydrate antigens defining tumor malignancy: basis for development of anti-cancer vaccines. *Advances in Experimental Medicine and Biology* **2001**, *491*, 369.
[17] T. Ariga, M. P. McDonald, R. K. Yu. Role of ganglioside metabolism in the pathogenesis of Alzheimer's disease. *Journal of Lipid Research* **2008**, *49*, 1157.
[18] W. R. Jung, H. G. Kim, K. L. Kim. Ganglioside GQ1b improves spatial learning and memory of rats as measured by the Y-maze and the Morris water maze tests. *Neuroscience Letters* **2008**, *439*, 220.
[19] M. L. DeMarco, R. J. Woods. Atomic-resolution conformational analysis of the GM3 ganglioside in a lipid bilayer and its implications for ganglioside-protein recognition at membrane surfaces. *Glycobiology* **2009**, *19*, 344.
[20] T. Feizi. Carbohydrate differentiation antigens: probable ligands for cell adhesion molecules. *Trends in Biochemical Sciences* **1991**, *16*, 84.
[21] K. N. Greenshields, S. K. Halstead, F. M. Zitman, S. Rinaldi, K. M. Brennan, C. O'Leary, L. H. Chamberlain, A. Easton, J. Roxburgh, J. Pediani, K. Furukawa, K. Furukawa, C. S. Goodyear, J. J. Plomp, H. J. Willison. The neuropathic potential of anti-GM1 autoantibodies is regulated by the local glycolipid environment in mice. *The Journal of Clinical Investigation* **2009**, *119*, 595.
[22] S. I. Hakomori. Bifunctional role of glycosphingolipids. Modulators for transmembrane signaling and mediators for cellular interactions. *The Journal of Biological Chemistry* **1990**, *265*, 18713.
[23] A. Wierzbicki, M. Gil, M. Ciesielski, R. A. Fenstermaker, Y. Kaneko, H. Rokita, J. T. Lau, D. Kozbor. Immunization with a mimotope of GD2 ganglioside induces CD8+ T cells that recognize cell adhesion molecules on tumor cells. *Journal of Immunology* **2008**, *181*, 6644.
[24] M. Kotani, I. Kawashima, H. Ozawa, T. Terashima, T. Tai. Differential distribution of major gangliosides in rat central nervous system detected by specific monoclonal antibodies. *Glycobiology* **1993**, *3*, 137.
[25] Ž. Vukelić, M. Zarei, J. Peter-Katalinić, A. D. Zamfir. Analysis of human hippocampus gangliosides by fully-automated chip-based nanoelectrospray tandem mass spectrometry. *Journal of Chromatography A* **2006**, *1130*, 238.
[26] A. D. Zamfir, Ž. Vukelić, L. Bîndila, J. Peter-Katalinić, R. Almeida, A. Sterling, M. Allen. Fully-automated chip-based nanoelectrospray

tandem mass spectrometry of gangliosides from human cerebellum. *Journal of the American Society for Mass Spectrometry* **2004**, *15*, 1649.

[27] Ž. Vukelić, S. Kalanj-Bognar, M. Froesch, L. Bîndila, B. Radić, M. Allen, J. Peter-Katalinić, A. D. Zamfir. Human gliosarcoma-associated ganglioside composition is complex and distinctive as evidenced by high-performance mass spectrometric determination and structural characterization. *Glycobiology* **2007**, *17*, 504.

[28] I. Meisen, J. Peter-Katalinić, J. Müthing. Discrimination of neolacto-series gangliosides with alpha2-3- and alpha2-6-linked N-acetylneuraminic acid by nanoelectrospray ionization low-energy collision-induced dissociation tandem quadrupole TOF MS. *Analytical Chemistry* **2003**, *75*, 5719.

[29] S. Kirsch, J. Müthing, J. Peter-Katalinić, L. Bîndila. Online nano-HPLC/ESI QTOF MS monitoring of alpha2-3 and alpha2-6 sialylation in granulocyte glycosphingolipidome. *Biological Chemistry* **2009**, *390*, 657.

[30] vZ. Vukelić, A. D. Zamfir, L. Bîndila, M. Froesch, J. Peter-Katalinić, S. Usuki, R. K. Yu. Screening and sequencing of complex sialylated and sulfated glycosphingolipid mixtures by negative ion electrospray Fourier transform ion cyclotron resonance mass spectrometry. *Journal of the American Society for Mass Spectrometry* **2005**, *16*, 571.

[31] A. D. Zamfir, Ž. Vukelić, A. Schneider, E. Sisu, N. Dinca, A. Ingendoh. A novel approach for ganglioside structural analysis based on electrospray multiple-stage mass spectrometry. *Journal of Biomolecular Techniques* **2007**, *18*, 188.

[32] A. Serb, C. Schiopu, C. Flangea, Ž. Vukelić, E. Sisu, L. Zagrean, A. D. Zamfir. High-throughput analysis of gangliosides in defined regions of fetal brain by fully automated chip-based nanoelectrospray ionization multistage mass spectrometry. *European Journal of Mass Spectrometry* **2009**, *15*, 541.

[33] R. Almeida, C. Mosoarca, M. Chirita, V. Udrescu, N. Dinca, Ž. Vukelić, M. Allen, A. D. Zamfir. *Analytical Biochemistry* **2008**, *378*, 52.

[34] A. H. Merrill Jr, M. C. Sullards, J. C. Allegood, S. Kelly, E. Wang. Sphingolipidomics: high-throughput, structure-specific, and quantitative analysis of sphingolipids by liquid chromatography tandem mass spectrometry. *Methods* **2005**, *36*, 207.

[35] Y. Chen, J. Allegood, Y. Liu, E. Wang, B. Cachón-González, T. M. Cox, A. H. Merrill Jr, M. C. Sullards. Imaging MALDI mass spectrometry using an oscillating capillary nebulizer matrix coating system and its application to analysis of lipids in brain from a mouse model of Tay-Sachs/Sandhoff disease. *Analytical Chemistry* **2008**, *80*, 2780.

[36] B. Domon, C. E. Costello. A systematic nomenclature for carbohydrate fragmentation in FAB-MS/MS spectra of glycoconjugates. *Glycoconjugate Journal* **1988**, *5*, 397.

[37] C. E. Costello, P. Juhasz, H. Perreault. New mass spectral approaches to ganglioside structure determination. *Progress in Brain Research* **1994**, *101*, 45.

[38] Q. Ann, J. Adams. Structure determination of ceramides and neutral glycosphingolipids by collisional activation of $[M+Li]^+$ ions. *Journal of the American Society for Mass Spectrometry* **1992**, *3*, 260.